Chemistry & Biology *13*, 409–419, April 2006 ©2006 Elsevier Ltd All rights reserved DOI 10.1016/j.chembiol.2006.02.005

Structure of the EntB Multidomain Nonribosomal Peptide Synthetase and Functional Analysis of Its Interaction with the EntE Adenylation Domain

Eric J. Drake,[1,2] David A. Nicolai,[1] and Andrew M. Gulick[1,2,*]
[1] Hautpman-Woodward Medical Research Institute
700 Ellicott Street
Buffalo, New York 14203
[2] Department of Structural Biology
The State University of New York at Buffalo
Buffalo, New York 14260

Summary

Nonribosomal peptide synthetases are modular proteins that operate in an assembly line fashion to bind, modify, and link amino acids. In the *E. coli* enterobactin NRPS system, the EntE adenylation domain catalyzes the transfer of a molecule of 2,3-dihydroxybenzoic acid to the pantetheine cofactor of EntB. We present here the crystal structure of the EntB protein that contains an N-terminal isochorismate lyase domain that functions in the synthesis of 2,3-dihydroxybenzoate and a C-terminal carrier protein domain. Functional analysis showed that the EntB-EntE interaction was surprisingly tolerant of a number of point mutations on the surface of EntB and EntE. Mutational studies on EntE support our previous hypothesis that members of the adenylate-forming family of enzymes adopt two distinct conformations to catalyze the two-step reactions.

Introduction

The nonribosomal peptide synthetases (NRPSs) are a family of modular proteins that catalyze the enzymatic synthesis of small peptides [1–3]. The secondary metabolites produced by the NRPS systems in bacteria and fungi include peptides with antibiotic, immunosuppressant, and anticancer activities, as well as some siderophores. The enzymatic synthesis of the NRPS products raises the possibility of engineering the NRPSs for the generation of catalysts that may synthesize peptides with novel activities [4].

Modular NRPSs contain multiple catalytic domains joined in a single protein that may be tens of thousands of residues in length. Usually, NRPSs contain one module for each amino acid that is incorporated into the final peptide. A minimal NRPS module contains two catalytic domains and a carrier protein domain, onto which the nascent peptide is attached during synthesis. The adenylation domain first activates the substrate through an adenylation reaction and then catalyzes the formation of a thioester between the acyl substrate and the phosphopantetheine (PPant) cofactor on the carrier protein domain. A condensation domain serves to catalyze peptide bond formation by transferring the amino acid from an upstream domain to an amino acid located on a downstream domain. Additional catalytic domains that exist in NRPSs include N-methylation and epimerization domains [1, 5]. The NRPS carrier protein domains contain a conserved serine that is posttranslationally modified by *holo*-ACP synthases with a PPant cofactor [6] and are similar to acyl carrier proteins involved in other cellular processes, including fatty acid biosynthesis and metabolism and polyketide biosynthesis.

E. coli contains a single NRPS system that is used in the synthesis of the siderophore enterobactin (Figure 1A). The enterobactin molecule contains three copies of a dipeptide of 2,3-dihydroxybenzoic acid (DHB) and serine [7]. The serine molecules form a trilactone ring between the carboxylate of one residue and the side chain hydroxyl of the next. Produced and secreted during iron-limiting conditions, the enterobactin molecule chelates an Fe^{3+} ion and is then taken up into the cell through the activity of the outer membrane transport protein FepA [7].

The enzymes involved in enterobactin synthesis are encoded by a six gene cluster (*entA–F)*. The DHB molecules are produced from chorismate by the activities of EntA, EntB, and EntC (Figure 1B). EntC first catalyzes the conversion of chorismate to isochorismate [8]. The isochorismate lyase (ICL) domain of EntB hydrolyzes the pyruvate group of isochorismate to form 2,3-dihydro-2,3-dihydroxybenzoate [9], which is converted to DHB by the activity of EntA, a 2,3-dihydro-2,3-dihydroxybenzoate dehydrogenase [10].

EntE, EntB, and EntF are NRPS enzymes that generate the enterobactin molecule from three molecules of DHB and three molecules of serine, by using energy derived from the hydrolysis of six ATP molecules. The EntE protein contains an adenylation domain specific for DHB (Figure 1C); EntE transfers the DHB molecule to the PPant cofactor that is bound to the aryl carrier protein (ArCP) domain of the EntB protein [11]. EntB is thus a two-domain NRPS that contains both the ICL and ArCP domains [12]. EntF contains the complete serine module and a C-terminal domain that catalyzes the formation of the trilactone ring [13, 14]. The enterobactin NRPS system, therefore, contains only two modules that work iteratively for the complete synthesis of the enterobactin molecule. The remaining protein of the enterobactin cluster, EntD, is a PPant transferase that adds the cofactors to the carrier protein domains of EntB and EntF [6, 12].

Structurally, the most well studied domain of the NRPS systems is the adenylation domain. The adenylation domains are part of a larger family of adenylate-forming enzymes that include firefly luciferase and acyl-CoA synthetases [15, 16]. All members of this family catalyze two-step reactions in which the first reaction is an adenylation step resulting in the formation of an acyl-AMP. NRPS adenylation domains and the acyl-CoA synthetases catalyze the formation of a thioester with either PPant or with CoA in the second half-reaction. In its second half-reaction, luciferase catalyzes an oxidative decarboxylation that results in an activated molecule that decomposes to emit light [17].

*Correspondence: gulick@hwi.buffalo.edu

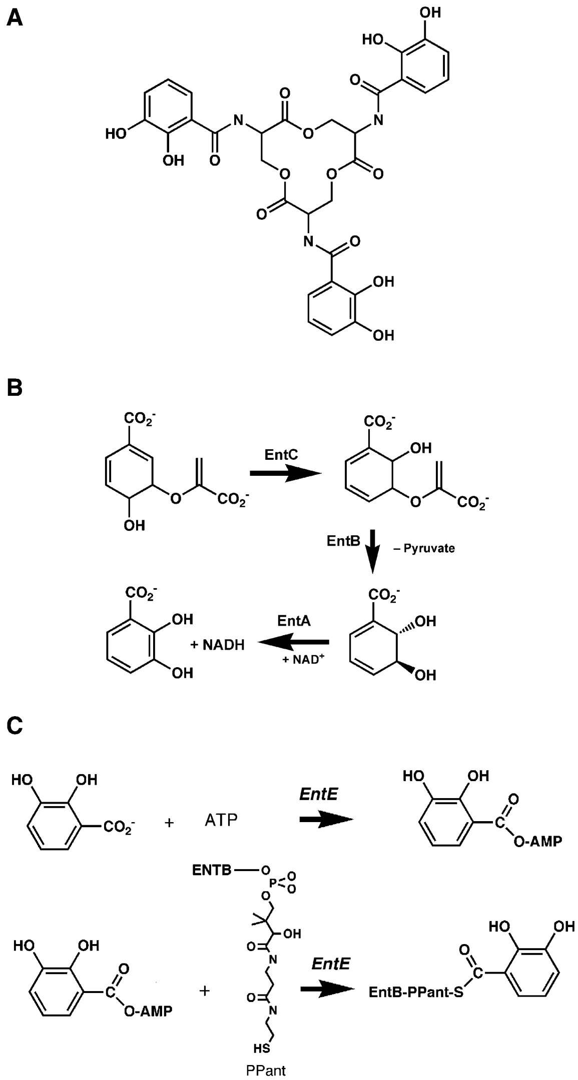

Figure 1. Enterobactin Synthesis

(A) Enterobactin consists of three DHB serine amides with ester linkages between serine side chain hydroxyls and carboxylates.

(B) The synthesis of DHB catalyzed by the sequential activities of EntC, the ICL domain of EntB, and EntA.

(C) The two-step reaction catalyzed by the EntE adenylation domain. The enzyme first catalyzes the formation of the DHB adenylate. In a second half-reaction, EntE transfers the DHB moiety to the PPant cofactor of the EntB ArCP domain.

Crystal structures exist for firefly luciferase [17], NRPS adenylation domains PheA [18] and DhbE [19], and several acyl- and aryl-CoA synthetases [20–23]. The enzymes contain a large N-terminal domain of 400–520 residues and a smaller C-terminal domain of ~120 residues. On the basis of structural and biochemical work, we have previously proposed [20, 21] that the members of this family adopt one conformation to catalyze the initial adenylation reaction. The C-terminal domain then rotates by ~140° to adopt a second conformation that is used to catalyze the second half-reaction. This conformational change, which we term domain alternation, reconfigures a single active site to catalyze the two half-reactions.

We have determined the crystal structure of the EntB protein and present here further insight into the activity of the NRPS adenylation domains. By using the EntB structure as well as structures of EntE homologs in adenylate- and thioester-forming conformations, we identified residues near the potential recognition interfaces of EntB and EntE. We have created a series of point mutations in EntB and tested them through kinetic analyses with EntE. We have also created a series of mutations in the EntE adenylation domain. Our results demonstrate that the EntE adenylation domain is remarkably tolerant of the point mutations in the EntB protein, and that a variety of single-residue replacements have little effect on the EntE-EntB interaction. These results also support the domain rotation proposal for adenylate-forming enzymes.

Results

Structure Determination of EntB

Crystallization of EntB was achieved through initial screening with sparse matrix conditions by using a wide variety of PEG- and salt-based precipitants [24, 25]. The structure of the two-domain EntB protein was determined by molecular replacement with PHASER [26, 27]. The search model was a single domain of the 207 residue 2-amino-2-deoxyisochorismate lyase (PhzD) protein [28]. PhzD, involved in phenazine biosynthesis, is 45.5% identical to the ICL domain of EntB. A molecular replacement solution was found with a dimer of ICL domains in the asymmetric unit. Gel filtration experiments demonstrated that the EntB forms a dimer in solution as well. Electron density for portions of the main helices of the ArCP domain was initially visible in difference density maps, and the connecting loops became apparent as model building and refinement proceeded. Crystallographic and refinement data statistics are shown in Table 1.

The final model for EntB contains 558 residues; subunit A is missing the N-terminal 4 residues and the C-terminal 2 residues, while subunit B is missing 3 residues from each terminus. Several residues have disordered side chains and have been modeled as alanines. Linking the N-terminal ICL domain with the C-terminal ArCP domain is the 5 residue sequence Pro-Ala-Pro-Ile-Pro. This extended peptide positions the C-terminal carrier protein domain away from the ICL domain (Figure 2A). The N-terminal domains of the two subunits of EntB superimpose with a root-mean-square (rms) deviation of 0.23 Å. Greater variability is observed with the C-terminal domain. The rms deviation derived from overlapping the two C-terminal domains is 0.32 Å; however, the C-terminal domains of the two subunits adopt different conformations relative to the N-terminal domain. The difference in the orientation between the two C-terminal domains is ~23°.

The N-terminal domain of EntB contains a central six-stranded parallel β sheet (Figure 2). On one side of the sheet are three α helices that form the subunit interface of the EntB dimer. On the opposite side of the sheet is a long α helix at residues Pro51-Asn71. A short single-turn helix caps the C-terminal ends of the β sheet. A small pocket forms between the core of the ICL domain and an interrupted helix at Asp85-Met94. The distal side of this

Table 1. Crystallographic and Refinement Data

Resolution	2.3 Å
Space group	$P2_12_12_1$
Unit cell	a = 50.9 Å, b = 82.3 Å, c = 164.7 Å
Matthews coefficient	2.64 $Å^3$/Da
R_{merge}[a]	5.9% (32.7%)
Completeness[a]	95.7% (76.8%)
I/σ[a]	18.1 (2.3)
Number of observations	115,010
Number of reflections	30,029
Resolution range	40.0–2.3 Å
R_{cryst}[a]	18.6% (25.2%)
R_{free}[a]	24.1% (32.2%)
Wilson B factor	47.8 $Å^2$
Average B factor, overall	45.0 $Å^2$
Average B factor, protein (N-term, chain A)[b]	42.2 $Å^2$, 42.2 $Å^2$
Average B factor, protein (C-term, chain A)[b]	53.9 $Å^2$, 55.1 $Å^2$
Average B factor, protein (N-term, chain B)[b]	41.7 $Å^2$, 42.2 $Å^2$
Average B factor, protein (C-term, chain B)[b]	52.8 $Å^2$, 52.0 $Å^2$
Average B factor, solvent (number of molecules)	44.3 $Å^2$ (229)
Average B factor, metal ions (number of ions)	51.7 $Å^2$ (10)
Average B factor, ethylene glycol (number of atoms)	59.9 $Å^2$ (4)
Rms deviation bond lengths, angles	0.011 Å, 1.245°

[a] Values for the highest-resolution shell (2.42–2.3 Å) are given in parentheses.
[b] Presented for main chain and side chain atoms, respectively.

helix makes hydrophobic interactions with the neighboring subunit, and Leu90 and Leu91 of one subunit interact with Trp24 and Tyr165 of the neighboring subunit of the dimer. A second set of interactions occurs between Met94 and Trp95 of one subunit and the methylene carbons of Lys21 and Arg196 of the neighboring subunit.

The ICL domain of the EntB protein is very similar to PhzD (Figure 3). The ICL domain and the PhzD molecule align with an rms deviation of 0.9 $Å^2$ over 195 Cα atoms. A comparison of the structures of the two proteins shows that there are two small loops that differ between the two proteins. The first, at residues Leu47–Cys50, results from a 2 residue insertion in EntB. This region of the protein is ~15 Å from the active site; there do not appear to be any long-range effects of this change, as the inner sphere of residues between the active site and this loop remains unchanged. The second structural difference occurs at residues Pro97–Gln106 of EntB. This loop immediately follows the interrupted helix described above that forms one wall of the active site. This structural change results in the movement of Gly98 of EntB in a direction positioning it slightly closer to the isochorismate ligand of PhzD. The distance from the Gly98 Cα position to the isochorismate aryl carboxylate is reduced from 3.9 Å in PhzD to 3.5 Å in EntB (Figure 3B). This change may reflect a difference between the liganded and unliganded structures. The PhzD structure was solved bound to isochorismate as well as in the unliganded form. The unliganded protein, however, contains a formate ion bound in the active site that approximates the position of the aryl carboxylate of isochorismate.

The ArCP domain of EntB is a typical acyl carrier protein domain consisting of four helices. The Ser245 residue of EntB, which is the site of addition of the cofactor, is positioned at the start of the second helix. The Ser245 residue is located on the ArCP face that points away from the ICL domain and is directed into solvent (Figure 2A). This location allows access of this site to the cofactor and to the EntE and EntF proteins with which it will interact. In the crystal lattice, the Ser245 side chain is positioned close to a symmetry-related molecule, and no electron density is observed for the PPant cofactor. Prior to structure solution by molecular replacement, attempts were made, without success, to grow crystals of selenomethionine (SeMet)-labeled EntB. SeMet-labeled protein was produced by the metabolic inhibition method [29] in minimal media, which, lacking sufficient iron, induced the EntD PPant transferase [30]. As the Ser245 side chain is in close proximity to a neighboring molecule in the crystal lattice, the *holo*-protein containing the PPant cofactor could not crystallize under the current conditions in the crystal form observed with the *apo*-protein.

A number of acyl, fatty acyl, and peptidyl carrier protein structures have been determined by crystallography and NMR [31–42]. There is considerable structural variation; however, nearly all structures contain the four main helices. A long loop joins helices 1 and 2, and the cofactor binding serine residue is located at the start of helix 2. Helices 1, 2, and 4 are similar in length and orientation, while helix 3 is shorter and nearly perpendicular to the other helices. A simple overlay of the Cα position of the different structures shows differences in the orientations of the helices and results in relatively high rms deviations of ~2.5 Å over the complete domains; this largely results from differences in the orientations of the main α helices. To best compare the structures of the different carrier protein domains, we used the program PROMOTIF [43] to determine the angles of interaction between different helices. For EntB, the angles between the helices were very similar to the values observed for the peptidyl carrier protein domain of the TycC3 NRPS protein [31]. The orientations of the helices show some consistency between three different classes of carrier protein domains: NRPS PCP domains, fatty acyl carrier protein domains, and ACP domains used in polyketide synthesis (Table 2). The angles observed between helices of the two NRPS proteins are more similar to those of the fatty acyl carrier protein domains than to the interhelical angles of the polyketide domains. Representative carrier proteins are shown in Figure 3C. We also compared the angles of the structures determined by crystallography with those determined by NMR and showed that the values did not correlate with experimental method (Table 2). Although the number of structures limits a full statistical correlation, the NRPS carrier proteins are more similar with respect to helical orientation to the acyl carrier proteins from primary metabolism than to the carrier protein domains involved in polyketide secondary metabolism.

Functional Analysis of EntB and EntE Mutants

By using our structure of EntB and prior structures of adenylate-forming enzymes [19–21] as a guide, we constructed point mutations in residues at the surfaces of

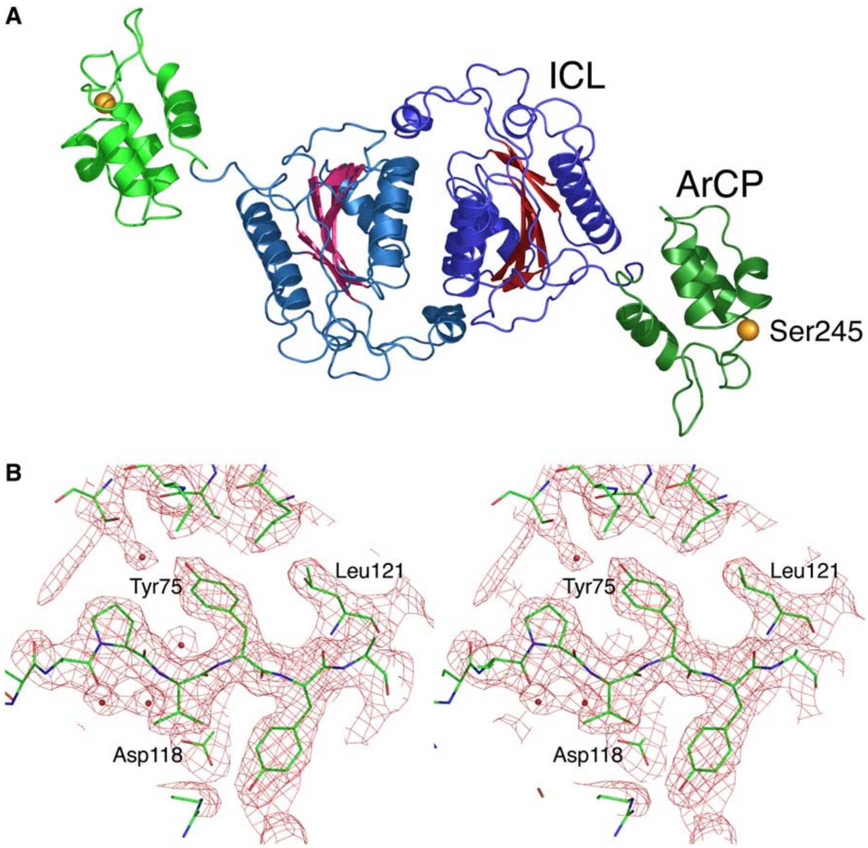

Figure 2. EntB Structure

(A) Ribbon diagram of the EntB dimer. The N-terminal ICL domains are shown with blue helices; the central sheet of the ICL domain is shown in red. The C-terminal ArCP domains are shown in green. The position of the cofactor binding Ser245 residue is represented with the gold sphere.
(B) Representative electron density. The electron density was calculated with coefficients of the form $2F_o - F_c$ and was contoured at 1σ.

EntB (Figures 4A and 4B) and EntE (Figure 4C) and tested these mutants for the intermolecular transfer of DHB from EntE to the EntB ArCP domain. Three loops (Leu225–Ser229, Ile239–Arg256, Asp261–Asn270) were identified on the surface of the ArCP domain near the PPant binding site of Ser245 (Figure 4B). Examination of the 32 residues that formed the interaction loops of EntB demonstrated that 10 of these residues were directed into the core of the protein and were unlikely to be involved in specific side chain interactions with EntE. Of the remaining 22 residues, we chose 9 residues for mutagenesis that might contribute to interactions with EntE; these residues were more centrally located near Ser245 and were also positioned where they might introduce charge or hydrophobic contacts toward the interface (Figure 4A). To determine if the residues formed specific interactions across the EntB/EntE interface, residues were replaced with amino acids that exhibited significantly different biochemical properties.

It was first necessary to produce the *holo*-EntB mutants and confirm that the mutations did not affect the ability of EntD to attach the PPant cofactor on the EntB mutants. We relied on the in vivo pantetheinylation of EntB by producing protein in minimal media. We used MALDI-TOF mass spectrometry to analyze cofactor content. Initially, two samples of wild-type protein were submitted, one purified from rich media and one purified from minimal media (Table 3). The difference in molecular weight between the two samples was 341.2 Da, representing the presence of the PPant cofactor on the protein produced in minimal media. To gauge the ability to use mass spectrometry as an analytical tool, a 50:50 mixture of the two samples was analyzed. The $[M+2H]^{2+}$ peak clearly distinguished the two samples and showed equal peak heights. Although mass spectrometry is not quantitative, we felt that this could be used to provide a rough estimate of the degree of cofactor addition. The remaining mutants were grown in M9 and subjected to mass spectrometric analysis. The cofactor was properly added by EntD to all mutants except one (Table 3). The remaining mutant, D244R, showed a mixture of *apo*- and *holo*-protein, with the peak of the *holo*-protein about 40% the height of the *apo*-protein peak. Three independent preparations of the D244R mutant were performed, and all generated the same result. This suggests that mutation of the Asp244 residue reduces the recognition of EntB by the EntD PPant transferase; however, a small fraction ($\sim$35% of the total EntB D244R protein produced) was still modified. In *E. coli* ACP, a homologous D35C mutant is also unable to be properly converted to the *holo*-ACP [44].

We then tested the ability of EntE to recognize the *holo*-EntB mutants and transfer the DHB molecule to

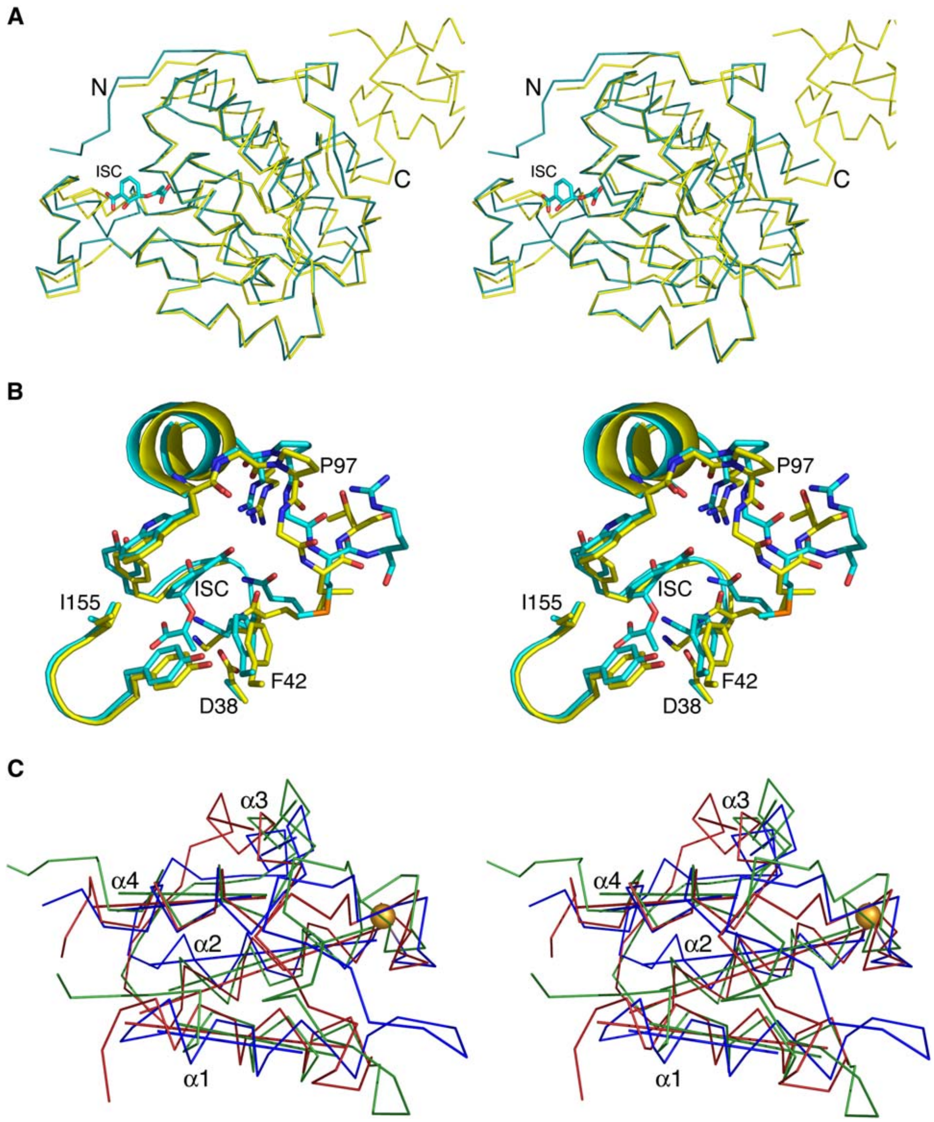

Figure 3. Structural Comparisons of EntB

(A) Cα superposition of EntB and PhzD. The EntB protein is shown in yellow, while the PhzD protein is shown in blue. Positioned in the active site is a molecule of isochorismate that was cocrystallized with PhzD (PDB code: 1NF8).

(B) Active site superposition of the PhzD protein (blue) with the EntB ICL domain (yellow). The loop at residues 97–106 of EntB is shown near the top of the figure. Note that the homolog of Asp37 in EntB is an aspartic acid in PhzD as well; however, this residue was mutated in the PhzD crystallization study to trap the enzyme with isochorismate.

(C) Stereorepresentation of the ACP domains. The EntB ArCP domain (shown in blue) is superimposed on the frenolicin polyketide synthase ACP (green, 1OR5) and the *E. coli* ACP (red, 1T8K). The yellow sphere is at Ser245 in EntB. The axes of the four main helices are shown for each domain.

the PPant cofactor of EntB by using a coupled AMP-formation assay. The S245A mutant and the wild-type EntB purified from cells grown in iron-rich media showed very limited activity as substrates for EntE. We then measured specific activity by using a single concentration of the mutant EntB proteins. The mutant enzymes all showed detectable activity with EntE; several served as better acceptor substrates than the wild-type EntB (Table 3).

Surprisingly, none of the dramatic mutations that we constructed hindered the specific activity; only two residues (Asp240 and Asp263) showed reductions in activity. While the D244R mutant showed only 13% activity, this assay was performed with the mixture of *apo*- and *holo*-protein and is thus difficult to interpret. We performed additional kinetic analyses with a subset of the mutant EntB enzymes that included the two mutant proteins that had the lowest specific activity and one of the mutants that showed elevated activity, F264E. Apparent kinetic constants were determined at constant concentrations of DHB and ATP and varying concentrations of the *holo*-EntB. As would be expected for residues located at the surface that may impact the recognition of EntB and EntE, there is only a minimal (less than 2-fold) effect on k_{cat}. In contrast, the two mutations with a mild impact on relative specific activity show increases in K_M.

Table 2. Interhelical Angles Observed in Different Carrier Protein Domains

	H1-H2 Angle	H1-H4 Angle	H2-H3 Angle	H2-H4 Angle	H3-H4 Angle
PKS (n = 3)	134.9 ± 4.7	118.2 ± 6.5	141.3 ± 1.6	−20.8 ± 3.6	148.4 ± 7.5
NRPS (n = 2)	141.8 ± 0.8	132.9 ± 5.0	113.4 ± 2.3	−24.2 ± 11.5	128.5 ± 1.6
ACP (n = 8)	141.8 ± 15.1	134.9 ± 15.4	126.2 ± 13.1	−23.5 ± 9.9	137.2 ± 13.7
NMR (n = 8)	138.1 ± 15.7	132.7 ± 17.3	131.0 ± 16.0	−21.9 ± 9.5	133.0 ± 13.7
X-ray (n = 5)	138.1 ± 11.1	127.5 ± 7.1	122.4 ± 10.6	−25.0 ± 5.9	143.3 ± 9.9

The average interhelical angles are listed for carrier proteins grouped either by experimental method or by biological function (PKS, polyketide synthase; NRPS, NRPS acyl or peptidyl carrier protein domains; ACP, acyl or fatty acyl carrier proteins). A total of 13 proteins were used in the analysis. These include three PKS ACP domains (1NQ4, oxytetracycline ACP from *S. rimosus* [39]; 1OR5, frenolicin ACP from *S. roseofulvus* [40]; 2AF8, actinorhodin ACP from *S. coelicolor* [35]), two NRPS carrier protein domains (1DNY, tyrocidin PCP domain from TycC from *B. brevis* [31]; ENTB, *E. coli* protein presented here), and eight acyl carrier protein domains (1L0H, 1T8K, and 1ACP, three independently determined structures of *E. coli* acyl carrier protein [32, 34, 38]; 1F80 and 1HY8, two independently determined structures of *B. subtilis* acyl carrier protein [36, 37]; 1DV5, D-alanyl carrier protein from *L. casei* [41]; 1KLP, acyl carrier protein from *M. tuberculosis* [42]; 1VKU, acyl carrier protein from *T. maritima*).

Mutational Analysis of EntE

We have proposed that members of the adenylate-forming family adopt two conformations to catalyze the two-step reaction [20, 21]. Starting with the crystal structure of DhbE [19], we created a model in which the C terminus of DhbE is in the thioester-forming conformation observed in the structure of acetyl-CoA synthetase bound to adenosine-5′-propylphosphate and CoA [21]. From this model, several residues were identified that project toward the surface of the DhbE protein in close proximity to the PPant binding tunnel. In the crystal structure of DhbE, these residues are more than 20 Å away from the active site in the adenylate bound conformation (Figure 4C). These residues were mutated to test for the ability to affect the EntB-EntE interaction.

EntE mutations made were R437D, K473D, R494D, and a double mutant containing R437D and K473D. Neither the wild-type nor any of the EntE mutants showed spontaneous hydrolysis of ATP to produce AMP in the absence of an EntB thiol acceptor (data not shown). Importantly, all four mutants were able to catalyze the exchange of radiolabeled pyrophosphate into ATP; thus, all four mutants were competent to catalyze the adenylation reaction (Table 3). In assays of the complete thioester-forming reaction, the K473D and R494D mutants had near wild-type activity, while R437D and the double mutant R437D/K473D were reduced to 10% and 3% specific activity, respectively, with the wild-type EntB substrate. These activity levels are comparable to the activities with wild-type EntE and the Ser245 mutant of EntB. Arg437 immediately precedes Gly438, a 100% conserved residue that is located on a loop that projects into the active site in the thioester-forming conformation observed in Acs [21]. These results therefore support domain alternation, as the ability of this mutation to affect the catalytic activity of the thioester-forming reaction specifically implies that this loop indeed rotates into the active site for the catalysis of the second half-reaction.

Discussion

We present here the structure of the two-domain NRPS protein EntB containing an N-terminal ICL domain and a C-terminal ArCP domain. The structure provides a view of the ICL catalytic active site. The EntB ICL domain is a member of a family of isochorismatase enzymes that may also serve as targets for inhibitor design [45]. There has been recent interest in the development of inhibitors of the enzymes involved in chorismate metabolism that may serve as leads for antibiotic development [46–48]. Also, the structure of a multidomain NRPS suggests how the domains are organized, and our structural and functional studies can provide additional clues to the interaction of NRPS domains.

The comparison of the ICL domain with the active site of PhzD [28] demonstrates strong conservation of important residues. The catalytic aspartic acid (Asp37 in EntB) is retained, as are the residues that form the mostly hydrophobic binding pocket (Phe42, Trp95, and Tyr126). Residues that interact with the aryl carboxylate (Gln79 and Arg88) are conserved, as is Lys123, which is positioned to interact with the pyruvate carboxylate. Indeed, the only inner shell residue of the active site that differs is the replacement of Val154 of PhzD with Ile155 in EntB (Figure 3B). Interestingly, this residue is located near the C4 position of the isochorismate ligand of the PhzD structure. The catalytic efficiency of PhzD is reduced by a factor of 50 with chorismate compared to isochorismate [28]. In contrast, the EntB protein displays a 10^3-fold decrease in catalytic efficiency for chorismate compared to isochorismate [9]. Our structural results suggest that the specificity reflects the inability of EntB to accommodate the hydroxyl at the C4 position of chorismate because of the replacement of Val154 in PhzD with Ile in EntB. Additional functional and structural studies of the ICL domain will further clarify the roles of individual active site residues.

Prior structural studies on NRPS proteins have been limited to single domains, either self-standing proteins like the adenylation domain DhbE [19] and the condensation domain VibH [49], or genetically truncated domains such as the phenylalanine-activating domain of GrsA [18], the PCP domain of TycC [31], and the cyclization/thioesterase domain of SrfA-C [50]. Although the two domains of EntB do not interact functionally, EntB serves as a suitable small model to demonstrate that some multidomain NRPS proteins retain sufficient structural rigidity for crystallization.

EntB uses a proline-rich linker to join the two domains. This peptide limits interactions between the two domains and maintains the active site of the N-terminal ICL domain and the PPant cofactor binding site of the ArCP domain at ∼45 Å from each other. Given the apparent functional and structural independence of these ICL and ArCP regions of the protein, one could ask

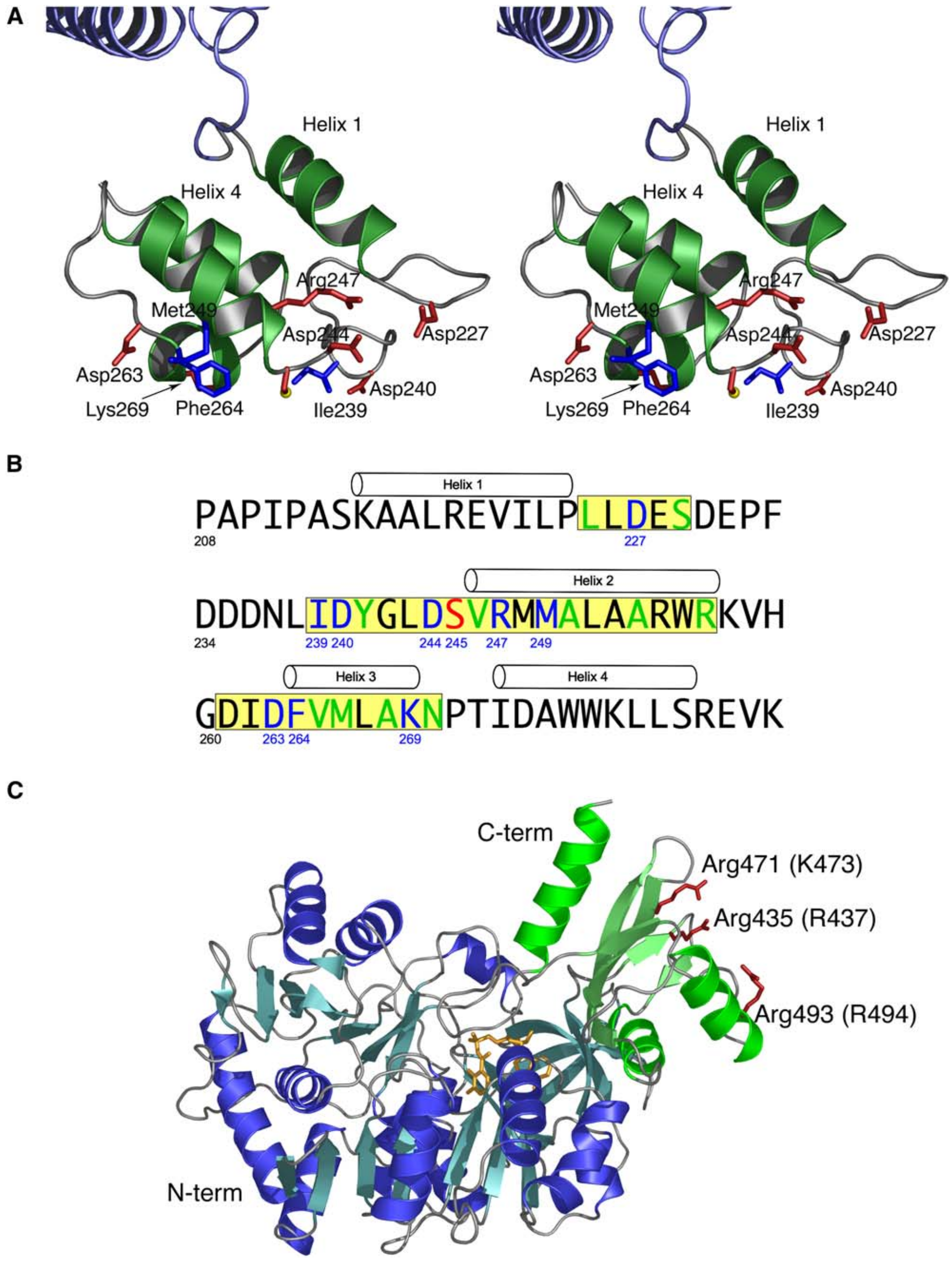

Figure 4. Location of EntB and EntE Mutations

(A) Mutations constructed in the EntB ArCP domain. A stereorepresentation of the EntB ArCP domain is shown. Ser245 is shown with the yellow sphere at the Oγ position. The remaining residues chosen for mutagenesis are shown in stick representation and are labeled. Hydrophobic residues are shown in blue, while charged or polar residues are shown in red.

(B) The sequence of the EntB ArCP domain is shown with locations of the four helices indicated. Highlighted in yellow are the three loops that form the surface of the ArCP domain around the Ser245 cofactor attachment site. Residues located on these loops that are directed to the center of the protein and therefore unlikely to be involved in interactions are black. The residues mutated in this study are shown in blue. The residues located on surface loops with side chains directed into solvent that were not mutated are green.

(C) Ribbon diagram of the DhbE protein crystallized in the presence of the DHB adenylate [19] in the proposed adenylate-forming conformation. The adenylate, shown in yellow, is located between the N-terminal (blue) and C-terminal (green) domains. Homologs of the three EntE residues mutated are shown. For two of the mutations, the residues are identical in DhbE and EntE (in parentheses); the remaining residue, Arg471 of DhbE, is a lysine in EntE.

why the two domains are expressed as a single protein. Perhaps this represents an extreme level of coregulation of these two elements in enterobactin synthesis. The synthesis of DHB from chorismate involves three steps catalyzed sequentially by EntC, EntB, and EntA. The reaction catalyzed by EntC is reversible; the K_{eq} for the reaction is 0.56 in favor of the chorismate-to-isochorismate direction [8]. The ICL step catalyzed by EntB is thus the committed step toward DHB production. By combining the ICL and ArCP domains, nature has

Table 3. Kinetic Analysis of the EntB-EntE Interaction

EntB Protein	Expected MW	Observed MW[a]	Relative Specific Activity[b]
Wild-type	33,091.7	33,100	1.00 ± 0.05
WT-rich media	32,750.3 (*apo*)	32,759	0.05 ± 0.01
S245A	32,734.3 (*apo*)	32,726	0.02 ± 0.01
D227R	33,132.6	33,119	3.64 ± 0.35
I239D	33,093.4	33,093	2.68 ± 0.13
D240R	33,132.6	33,121	0.80 ± 0.11
D244R *apo*[c]	32,791.4	32,781	0.13 ± 0.02
D244R *holo*[c]	33,132.6	33,123	—
R247E	33,064.4	33,057	2.15 ± 0.02
M249E	33,089.4	33,092	1.04 ± 0.07
D263R	33,132.6	33,117	0.66 ± 0.01
F264E	33,073.4	33,070	3.15 ± 0.26
K269E	33,092.4	33,090	2.42 ± 0.37
EntB Protein	**EntE K_M (EntB) (μM)**	**EntE k_{cat} (sec^{-1})**	**EntE k_{cat}/K_M (sec^{-1} μM^{-1})**
Wild-type	23.3 ± 4.4	5.94 ± 0.25	0.26 ± 0.05
D240R	181.5 ± 14.0	9.54 ± 0.33	0.05 ± 0.01
D263R	64.8 ± 13.2	7.48 ± 0.63	0.12 ± 0.03
F264E	31.8 ± 5.1	10.30 ± 0.19	0.32 ± 0.05
EntE Mutant	**Relative EntE Specific Activity (Complete Reaction)[b]**		**Relative PPi-Exchange Activity[b]**
Wild-type	1.00 ± 0.05		1.00 ± 0.11
R437D	0.10 ± 0.01		0.94 ± 0.15
K473D	0.87 ± 0.08		0.87 ± 0.17
R494D	0.92 ± 0.11		0.90 ± 0.22
R437D/K473D	0.03 ± 0.01		0.84 ± 0.12

[a] Molecular weight was observed by MALDI-TOF Mass spectrometry as described in the Experimental Procedures.
[b] Activity was calculated for the EntE-catalyzed reactions by using the complete reaction (measuring AMP production with the coupled assay) or the adenylation reaction by using PPi-exchange. Results are expressed relative to wild-type.
[c] Two peaks were observed in the MS analysis of the D244R mutant, one corresponding to the *holo*-protein and one corresponding to the *apo*-protein. The relative kinetic activity represents the activity observed with the mixture of *apo*- and *holo*-proteins.

evolved to ensure the availability of the EntB ArCP domain when DHB is produced.

A long-standing goal, with obvious technical challenges, is to determine the structure of even larger multidomain NRPSs. Until such studies are successful, structures of individual domains will continue to provide details that can be used in the generation of models for the interaction of neighboring domains. The creation of such models will benefit from the limitations imposed by available structural and biochemical data. For example, the generation of a model for the interaction of the EntE adenylation domain and the EntB ArCP domain is constrained by the lengths of linker peptides that occur between fused adenylation and carrier protein domains. To identify the linker region between the adenylation and PCP domains, the C-terminal Ala536 of EntE was taken as the C terminus of the adenylation domain, and Ile211 of EntB was taken as the N-terminal residue of the PCP domain. Alignments of multiple adenylation domain carrier protein domain sequences showed that the linker between these two residues is as short as 6 residues. Assuming an extended conformation of this region of the protein, the distance between Ile211 of EntB and Ala536 of EntE in the thioester-forming complex is, at most, 20–25 Å.

As efforts to engineer novel NRPS systems continue, it will be necessary to understand how NRPS domains interact sequentially during catalysis. Our results demonstrate that the EntB-EntE interaction is remarkably tolerant to the single point mutations that we have constructed near the Ser245 cofactor binding position. Of the nine mutations generated in EntB, five show elevated specific activity when compared with wild-type EntB. This observation that the EntB sequence is not optimized for interaction with EntE may reflect the evolutionary demands placed on the carrier protein domains, which must interact with multiple protein partners. Mutations that result in elevated binding affinity between EntB and EntE may not provide a sufficient selective advantage if they are detrimental to interactions between EntB and either of its other partners, EntF or EntD. Alternatively, the carrier protein domains may have evolved to interact with only moderate affinity with any one partner as a mechanism to retain the ability to migrate from one protein partner to the next.

Significance

NRPSs are involved in the synthesis of small peptides that can have antibiotic, immunosuppressant, or other activities. The modular nature of the NRPSs makes them suitable targets for engineering through the modification of substrate binding pockets or through domain or module rearrangements. The ability to reposition domains, however, requires an understanding of the nature of the interactions between specific domains to avoid the juxtaposition of incompatible domains. The crystal structure of the EntB protein provides insight into the nature of an NRPS two-domain protein and demonstrates that the ArCP domain protrudes from the ICL domain in a way that enables it to interact with EntE and the condensation domain of EntF. Our functional analysis suggests that the nature of the interaction of EntB with EntE is rather

promiscuous, and that multiple single-residue point mutations have little effect on the ability of EntE to recognize EntB. Our structural results also demonstrate that the NRPS carrier protein domains may share more overall structural similarities with ACP domains involved in fatty acid synthesis than with the ACP domains of polyketide biosynthesis. The mutagenesis studies presented here support the domain alternation hypothesis, which suggests that adenylation domains will undergo a 140° domain rotation to catalyze the two sequential chemical steps. This feature, together with consideration of the lengths of interdomain linkers, will assist in the modeling of the interaction of adenylation domains with carrier protein domains in both inter- and intramolecular transfers of acyl substrates.

Experimental Procedures

Cloning, Expression, and Purification of EntE

The *entE* gene was cloned from *E. coli* JM109 DNA by PCR. Template DNA was prepared by boiling 10 μl of an overnight culture in 90 μl water for 5 min. The primers used for PCR were 5′-CCAGTGCA TATGAGCATTCCATTCACCCG-3′ and 5′-CCACTCGAGTCAGGCT GATGCGCGTGAC-3′. The 1.6 kB gene product was cloned initially into pGEM7z and then subcloned into a modified pET15b plasmid that contained a TEV protease site [51]. All sequences were confirmed by DNA sequencing. This plasmid was used for expression in BL21(DE3) cells. Cultures of cells were grown to an OD_{600} of ~0.6 at 37°C and were induced with 0.5 mM IPTG for 3 hr. Cells were lysed by sonication in a buffer containing 40 mM HEPES (pH 7.5 at 4°C), 150 mM KCl, 20 mM imidazole, and 0.2 mM tris-(carboxyethyl)phosphine (TCEP). Protein was purified by metal chelate affinity chromatography. The column was washed with 50 mM imidazole, followed by elution of tagged EntE with the lysis buffer containing 300 mM imidazole. The purified protein was dialyzed into cleavage buffer (50 mM N-2-hydroxyethylpiperizaine-N′-3-propanesulfonic acid [HEPPS] [pH 8.0 at 4°C], 150 mM NaCl, 0.5 mM EDTA, and 0.2 mM TCEP). TEV protease (~0.3 mg) was added to the tagged protein and allowed to react overnight at 4°C in the dialysis bag. The cleaved protein was passed over a metal chelate column, and the untagged protein was collected from the flowthrough. The final protein was dialyzed into 10 mM HEPES (pH 7.5 at 4°C), 0.2 mM TCEP, and 1 mM NaN_3. From 1 L of cells, ~45 mg protein was obtained. This protein was frozen by pipetting directly into liquid nitrogen and was stored at −80°C.

Cloning and Expression of EntB

The PCR primers used to clone *entB* were 5′-CCAGTGCATATGGC TATTCCAAAATTACAG-3′ and 5′-CCACTCGAGTTATTTCACCTCGC GGGAG-3′. The amplified gene was cloned into pGEM7z and then pET15bTEV. Protein expression in BL21(DE3) cells was induced with 0.5 mM IPTG overnight at 16°C. Purification was again obtained by two metal chelate chromatography steps separated by removal of the His tag with TEV. Lysis buffer (50 mM HEPES [pH 7.5 at 4°C], 150 mM NaCl, 0.2 mM TCEP, 10 mM imidazole) and elution buffer (50 mM HEPES [pH 7.5 at 4°C], 150 mM NaCl, 0.2 mM TCEP, 300 mM imidazole) were used for purification. The TEV cleavage buffer was as described for EntE. The final dialysis buffer contained 20 mM HEPES (pH 7.5 at 4°C), 50 mM NaCl, and 0.2 mM TCEP.

Expression of *Holo*-EntB

Attempts to grow crystals of SeMet-labeled protein, produced by metabolic inhibition in M9 minimal media, were never successful. Once the final structure was obtained by using crystals grown of native protein, it was discovered that Ser245 was clearly unmodified with the PPant cofactor. We reasoned that production of SeMet protein by growth in minimal media induced the host *ent* operon, resulting in the production of the EntD PPant transferase. The presence of the cofactor on Ser245 sterically hinders lattice packing and provides an explanation for why we were unable to crystallize the SeMet protein. *holo*-EntB, used for functional assays, was produced by growing cells in M9 minimal media supplemented with 0.18% glucose, 148 μM thiamine, and 50 μg/ml ampicillin. Reproducing the protocol that we had used to make SeMet-labeled protein, an amino acid cocktail was added to a final concentration of 27 μM lysine, 42 μM threonine, 30 μM phenylalanine, 19 μM leucine, 19 μM isoleucine, 21 μM valine, and 17 μM methionine 30 min prior to induction. The purification was the same as for wild-type protein. EntB samples were submitted to the Roswell Park Cancer Institute Proteomics Facility for mass spectrometry analysis with a Waters Micromass MALDI Micro MX mass spectrometer with 10 mg/ml sinapinic acid as the matrix. The molecular weight was calculated from the $[M+2H]^{2+}$ ions because of improved resolution.

Crystallization of EntB and Structure Determination

Crystals of EntB were grown at 14°C by hanging drop vapor diffusion with a precipitant containing 10%–15% methyl ether PEG 5000, 0.7–0.9 M $MgCl_2$, 10% ethylene glycol, and 50 mM HEPPS (pH 8.0). The crystals tended to be highly anisotropic, and multiple additives were tested to improve the diffraction. The best crystals were obtained by transferring the crystals from mother liquor to solutions containing $CaCl_2$ instead of $MgCl_2$. The crystals were simultaneously cryoprotected by increasing the concentration of ethylene glycol to 22%. Crystals were soaked for 9 min in 15% MePEG5000, 0.75 M $CaCl_2$, 11% ethylene glycol, 50 mM HEPPS (pH 8.0), and they were soaked for 8 min in the same solution with 22% ethylene glycol. Diffraction data were collected at −170°C by using a Rigaku RU-H3RHB rotating anode, Osmic Max-Flux confocal focusing mirrors, and an R-axis IV image plate. Diffraction images were processed with MOSFILM [52], merged with SCALA, and converted to structure factors with TRUNCATE of the CCP4 software suite [53].

The EntB structure was determined by molecular replacement by using a single subunit of the PhzD protein [28] (PDB code: 1NF9) as a search model. The program PHASER [27] was used to identify the location of the two molecules in the asymmetric unit. Refinement of the initial solution with REFMAC resulted in a model with a crystallographic R_{cryst} of 38.3% (R_{free} of 42.5%). Statistics for data collection and refinement are presented in Table 1. Representative electron density is shown in Figure 2B.

Mutagenesis of EntB and EntE

Site-directed mutagenesis was carried out by using the QuikChange Mutagenesis Kit (Stratagene) and by following the manufacturer's protocol. Oligonucleotides were designed to contain the desired point mutation plus additional silent mutations to validate the reaction by using a restriction digest. PCR was performed under the following conditions: denaturation at 95°C for 30 s, followed by 16 cycles of denaturation at 95°C for 30 s, annealing at 55°C for 1 min, and extension at 68°C for 10 min. Plasmid DNA was screened for the inserted silent restriction change, and the entire coding region was sequenced to confirm the introduction of the desired mutation only.

Assay for Adenylation Activity of EntE with Wild-Type or Mutant EntB Proteins

Specific activity was determined by using an $NADH^+$ consumption assay monitored at OD_{340}. Standard assays contained 50 mM HEPES buffer (pH 7.5), 5 mM $MgCl_2$, 1 mM TCEP, 1 mM ATP, 2 mM DHB, 3 mM phosphoenolpyruvate, 4 U myokinase, 4.5 U pyruvate kinase, 6.5 U lactate dehydrogenase, and 250 μM $NADH^+$. EntE and EntB proteins were introduced into the reaction at 2 μM and 60 μM, respectively. Specific activity was calculated from the linear disappearance of $NADH^+$, monitored for 180 s or until the absorbance due to $NADH^+$ reached a plateau (due to covalent modification of all *holo*-EntB). Wild-type activity was 0.18 μmol/min/mg EntE. To determine apparent kinetic constants, the EntB concentration was varied from 10 to 90 μM. The program DYNAFIT [54] was used to determine kinetic constants from the initial velocities.

Pyrophosphate Exchange Assay

The pyrophosphate exchange assay was performed by using standard techniques [11, 15]. In this assay, EntE is allowed to catalyze the initial adenylation half-reaction in the absence of a thiol acceptor molecule; during the reverse reaction, radiolabeled PPi is incorporated into ATP. Specifically, 1.0 μM EntE was added to 2 mM ATP, 0.2 mM NaPPi, 50 mM HEPES (pH 8.0), 100 mM NaCl, 10 mM

$MgCl_2$, 0.15 μCi ^{32}P-PPi, and 5 mM DHB. Reactions (100 μl) were incubated for 10 min at 37°C, then quenched with 0.5 ml 1.2% charcoal, 0.1 M unlabeled PPi, and 0.35 M perchloric acid. The charcoal was pelleted, washed twice with 1 ml H_2O, and resuspended in 0.5 ml H_2O for scintillation counting. Five replicate assays were performed for each protein; results were recorded as μmol radiolabeled ATP incorporated per min per mg of enzyme. Wild-type activity was 210 μmol radiolabeled ATP produced per min per mg of EntE.

Acknowledgments

We would like to thank Kristen M. Homick for assistance with cloning *entE* and *entB* and Jeff Mocny for assistance in crystallizing the EntB protein. We would also like to thank Drs. Young-Mee Park, Rama Dey-Rao, and Liguo Song of the Roswell Park Proteomics facility for the mass spectrometry analysis. This research was supported by National Institutes of Health Grant GM-068440 (to A.M.G.) and start-up funds from the John R. Oishei Foundation.

Received: July 13, 2005
Revised: January 30, 2006
Accepted: February 10, 2006
Published: April 21, 2006

References

1. Challis, G.L., and Naismith, J.H. (2004). Structural aspects of non-ribosomal peptide biosynthesis. Curr. Opin. Struct. Biol. *14*, 748–756.
2. Sieber, S.A., and Marahiel, M.A. (2005). Molecular mechanisms underlying nonribosomal peptide synthesis: approaches to new antibiotics. Chem. Rev. *105*, 715–738.
3. Walsh, C.T. (2004). Polyketide and nonribosomal peptide antibiotics: modularity and versatility. Science *303*, 1805–1810.
4. Mootz, H.D., and Marahiel, M.A. (1999). Design and application of multimodular peptide synthetases. Curr. Opin. Biotechnol. *10*, 341–348.
5. Marahiel, M.A., Stachelhaus, T., and Mootz, H.D. (1997). Modular peptide synthetases involved in nonribosomal peptide synthesis. Chem. Rev. *97*, 2651–2674.
6. Lambalot, R.H., Gehring, A.M., Flugel, R.S., Zuber, P., LaCelle, M., Marahiel, M.A., Reid, R., Khosla, C., and Walsh, C.T. (1996). A new enzyme superfamily - the phosphopantetheinyl transferases. Chem. Biol. *3*, 923–936.
7. Raymond, K.N., Dertz, E.A., and Kim, S.S. (2003). Enterobactin: an archetype for microbial iron transport. Proc. Natl. Acad. Sci. USA *100*, 3584–3588.
8. Liu, J., Quinn, N., Berchtold, G.A., and Walsh, C.T. (1990). Overexpression, purification, and characterization of isochorismate synthase (EntC), the first enzyme involved in the biosynthesis of enterobactin from chorismate. Biochemistry *29*, 1417–1425.
9. Rusnak, F., Liu, J., Quinn, N., Berchtold, G.A., and Walsh, C.T. (1990). Subcloning of the enterobactin biosynthetic gene entB: expression, purification, characterization, and substrate specificity of isochorismatase. Biochemistry *29*, 1425–1435.
10. Liu, J., Duncan, K., and Walsh, C.T. (1989). Nucleotide sequence of a cluster of *Escherichia coli* enterobactin biosynthesis genes: identification of entA and purification of its product 2,3-dihydro-2,3-dihydroxybenzoate dehydrogenase. J. Bacteriol. *171*, 791–798.
11. Rusnak, F., Faraci, W.S., and Walsh, C.T. (1989). Subcloning, expression, and purification of the enterobactin biosynthetic enzyme 2,3-dihydroxybenzoate-AMP ligase: demonstration of enzyme-bound (2,3-dihydroxybenzoyl)adenylate product. Biochemistry *28*, 6827–6835.
12. Gehring, A.M., Bradley, K.A., and Walsh, C.T. (1997). Enterobactin biosynthesis in *Escherichia coli*: isochorismate lyase (EntB) is a bifunctional enzyme that is phosphopantetheinylated by EntD and then acylated by EntE using ATP and 2,3-dihydroxybenzoate. Biochemistry *36*, 8495–8503.
13. Gehring, A.M., Mori, I., and Walsh, C.T. (1998). Reconstitution and characterization of the *Escherichia coli* enterobactin synthetase from EntB, EntE, and EntF. Biochemistry *37*, 2648–2659.
14. Shaw-Reid, C.A., Kelleher, N.L., Losey, H.C., Gehring, A.M., Berg, C., and Walsh, C.T. (1999). Assembly line enzymology by multimodular nonribosomal peptide synthetases: the thioesterase domain of *E. coli* EntF catalyzes both elongation and cyclolactonization. Chem. Biol. *6*, 385–400.
15. Babbitt, P.C., Kenyon, G.L., Martin, B.M., Charest, H., Slyvestre, M., Scholten, J.D., Chang, K.H., Liang, P.H., and Dunaway-Mariano, D. (1992). Ancestry of the 4-chlorobenzoate dehalogenase: analysis of amino acid sequence identities among families of acyl:adenyl ligases, enoyl-CoA hydratases/isomerases, and acyl-CoA thioesterases. Biochemistry *31*, 5594–5604.
16. Chang, K.H., Xiang, H., and Dunaway-Mariano, D. (1997). Acyl-adenylate motif of the acyl-adenylate/thioester-forming enzyme superfamily: a site-directed mutagenesis study with the *Pseudomonas sp*. strain CBS3 4-chlorobenzoate:coenzyme A ligase. Biochemistry *36*, 15650–15659.
17. Conti, E., Franks, N.P., and Brick, P. (1996). Crystal structure of firefly luciferase throws light on a superfamily of adenylate-forming enzymes. Structure *4*, 287–298.
18. Conti, E., Stachelhaus, T., Marahiel, M.A., and Brick, P. (1997). Structural basis for the activation of phenylalanine in the nonribosomal biosynthesis of gramicidin S. EMBO J. *16*, 4174–4183.
19. May, J.J., Kessler, N., Marahiel, M.A., and Stubbs, M.T. (2002). Crystal structure of DhbE, an archetype for aryl acid activating domains of modular nonribosomal peptide synthetases. Proc. Natl. Acad. Sci. USA *99*, 12120–12125.
20. Gulick, A.M., Lu, X., and Dunaway-Mariano, D. (2004). Crystal structure of 4-chlorobenzoate:CoA ligase/synthetase in the unliganded and aryl substrate-bound states. Biochemistry *43*, 8670–8679.
21. Gulick, A.M., Starai, V.J., Horswill, A.R., Homick, K.M., and Escalante-Semerena, J.C. (2003). The 1.75 Å crystal structure of acetyl-CoA synthetase bound to adenosine-5′-propylphosphate and coenzyme A. Biochemistry *42*, 2866–2873.
22. Hisanaga, Y., Ago, H., Nakagawa, N., Hamada, K., Ida, K., Yamamoto, M., Hori, T., Arii, Y., Sugahara, M., Kuramitsu, S., et al. (2004). Structural basis of the substrate-specific two-step catalysis of long chain fatty acyl-CoA synthetase dimer. J. Biol. Chem. *279*, 31717–31726.
23. Jogl, G., and Tong, L. (2004). Crystal structure of yeast acetyl-coenzyme A synthetase in complex with AMP. Biochemistry *43*, 1425–1431.
24. Carter, C.W., Jr., and Carter, C.W. (1979). Protein crystallization using incomplete factorial experiments. J. Biol. Chem. *254*, 12219–12223.
25. Jancarik, J., and Kim, S.-H. (1991). Sparse matrix sampling: a screening method for crystallization of proteins. J. Appl. Crystallogr. *24*, 409–411.
26. Read, R.J. (2001). Pushing the boundaries of molecular replacement with maximum likelihood. Acta Crystallogr. D Biol. Crystallogr. *57*, 1373–1382.
27. Storoni, L.C., McCoy, A.J., and Read, R.J. (2004). Likelihood-enhanced fast rotation functions. Acta Crystallogr. D Biol. Crystallogr. *60*, 432–438.
28. Parsons, J.F., Calabrese, K., Eisenstein, E., and Ladner, J.E. (2003). Structure and mechanism of *Pseudomonas aeruginosa* PhzD, an isochorismatase from the phenazine biosynthetic pathway. Biochemistry *42*, 5684–5693.
29. Doubliè, S. (1997). Preparation of selenomethionyl proteins for phase determination. Methods Enzymol. *276*, 523–530.
30. Rusnak, F., Sakaitani, M., Drueckhammer, D., Reichert, J., and Walsh, C.T. (1991). Biosynthesis of the *Escherichia coli* siderophore enterobactin: sequence of the entF gene, expression and purification of EntF, and analysis of covalent phosphopantetheine. Biochemistry *30*, 2916–2927.
31. Weber, T., Baumgartner, R., Renner, C., Marahiel, M.A., and Holak, T.A. (2000). Solution structure of PCP, a prototype for the peptidyl carrier domains of modular peptide synthetases. Struct. Fold. Des. *8*, 407–418.
32. Roujeinikova, A., Baldock, C., Simon, W.J., Gilroy, J., Baker, P.J., Stuitje, A.R., Rice, D.W., Slabas, A.R., and Rafferty, J.B. (2002). X-ray crystallographic studies on butyryl-ACP reveal flexibility of the structure around a putative acyl chain binding site. Structure (Camb) *10*, 825–835.

33. Holak, T.A., Nilges, M., Prestegard, J.H., Gronenborn, A.M., and Clore, G.M. (1988). Three-dimensional structure of acyl carrier protein in solution determined by nuclear magnetic resonance and the combined use of dynamical simulated annealing and distance geometry. Eur. J. Biochem. *175*, 9–15.
34. Kim, Y., and Prestegard, J.H. (1990). Refinement of the NMR structures for acyl carrier protein with scalar coupling data. Proteins *8*, 377–385.
35. Crump, M.P., Crosby, J., Dempsey, C.E., Parkinson, J.A., Murray, M., Hopwood, D.A., and Simpson, T.J. (1997). Solution structure of the actinorhodin polyketide synthase acyl carrier protein from *Streptomyces coelicolor* A3(2). Biochemistry *36*, 6000–6008.
36. Xu, G.Y., Tam, A., Lin, L., Hixon, J., Fritz, C.C., and Powers, R. (2001). Solution structure of *B. subtilis* acyl carrier protein. Structure (Camb) *9*, 277–287.
37. Parris, K.D., Lin, L., Tam, A., Mathew, R., Hixon, J., Stahl, M., Fritz, C.C., Seehra, J., and Somers, W.S. (2000). Crystal structures of substrate binding to *Bacillus subtilis* holo-(acyl carrier protein) synthase reveal a novel trimeric arrangement of molecules resulting in three active sites. Struct. Fold. Des. *8*, 883–895.
38. Qui, X., and Janson, C.A. (2004). Structure of apo acyl carrier protein and a proposal to engineer protein crystallization through metal ions. Acta Crystallogr. D Biol. Crystallogr. *60*, 1545–1554.
39. Findlow, S.C., Winsor, C., Simpson, T.J., Crosby, J., and Crump, M.P. (2003). Solution structure and dynamics of oxytetracycline polyketide synthase acyl carrier protein from *Streptomyces rimosus*. Biochemistry *42*, 8423–8433.
40. Li, Q., Khosla, C., Puglisi, J.D., and Liu, C.W. (2003). Solution structure and backbone dynamics of the holo form of the frenolicin acyl carrier protein. Biochemistry *42*, 4648–4657.
41. Volkman, B.F., Zhang, Q., Debabov, D.V., Rivera, E., Kresheck, G.C., and Neuhaus, F.C. (2001). Biosynthesis of D-alanyl-lipoteichoic acid: the tertiary structure of apo-D-alanyl carrier protein. Biochemistry *40*, 7964–7972.
42. Wong, H.C., Liu, G., Zhang, Y.M., Rock, C.O., and Zheng, J. (2002). The solution structure of acyl carrier protein from *Mycobacterium tuberculosis*. J. Biol. Chem. *277*, 15874–15880.
43. Hutchinson, E.G., and Thornton, J.M. (1996). PROMOTIF–a program to identify and analyze structural motifs in proteins. Protein Sci. *5*, 212–220.
44. Worsham, L.M., Earls, L., Jolly, C., Langston, K.G., Trent, M.S., and Ernst-Fonberg, M.L. (2003). Amino acid residues of *Escherichia coli* acyl carrier protein involved in heterologous protein interactions. Biochemistry *42*, 167–176.
45. Caruthers, J., Zucker, F., Worthey, E., Myler, P.J., Buckner, F., Van Voorhuis, W., Mehlin, C., Boni, E., Feist, T., Luft, J., et al. (2005). Crystal structures and proposed structural/functional classification of three protozoan proteins from the isochorismatase superfamily. Protein Sci. *14*, 2887–2894.
46. Kerbarh, O., Bulloch, E.M., Payne, R.J., Sahr, T., Rebeille, F., and Abell, C. (2005). Mechanistic and inhibition studies of chorismate-utilizing enzymes. Biochem. Soc. Trans. *33*, 763–766.
47. Payne, R.J., Kerbarh, O., Miguel, R.N., Abell, A.D., and Abell, C. (2005). Inhibition studies on salicylate synthase. Org. Biomol. Chem. *3*, 1825–1827.
48. Ferreras, J.A., Ryu, J.S., Di Lello, F., Tan, D.S., and Quadri, L.E. (2005). Small-molecule inhibition of siderophore biosynthesis in *Mycobacterium tuberculosis* and *Yersinia pestis*. Nat. Chem. Biol. *1*, 29–32.
49. Keating, T.A., Marshall, C.G., Walsh, C.T., and Keating, A.E. (2002). The structure of VibH represents nonribosomal peptide synthetase condensation, cyclization and epimerization domains. Nat. Struct. Biol. *9*, 522–526.
50. Bruner, S.D., Weber, T., Kohli, R.M., Schwarzer, D., Marahiel, M.A., Walsh, C.T., and Stubbs, M.T. (2002). Structural basis for the cyclization of the lipopeptide antibiotic surfactin by the thioesterase domain SrfTE. Structure (Camb) *10*, 301–310.
51. Kapust, R.B., Tozser, J., Fox, J.D., Anderson, D.E., Cherry, S., Copeland, T.D., and Waugh, D.S. (2001). Tobacco etch virus protease: mechanism of autolysis and rational design of stable mutants with wild-type catalytic proficiency. Protein Eng. *14*, 993–1000.
52. Leslie, A.G.W. (1992). Recent changes to the MOSFLM package for processing film and image plate data. In Joint CCP4 + ESF-EAMCB Newsletter on Protein Crystallography, Volume 26.
53. CCP4 (Collaborative Computational Project, Number 4) (1994). The CCP4 suite: programs for protein crystallography. Acta Crystallogr. D Biol. Crystallogr. *50*, 760–763.
54. Kuzmic, P. (1996). Program DYNAFIT for the analysis of enzyme kinetic data: application to HIV proteinase. Anal. Biochem. *237*, 260–273.

Accession Numbers

Atomic coordinates and structure factors for EntB have been deposited in the Protein Data Bank (PDB code: 2FQ1).